

Geochemistry, Geophysics, Geosystems

RESEARCH ARTICLE

10.1002/2015GC006176

Key Points:

- New 3-D versus model of central-Europe crust, that correlates well with existing vp models
- The model is coherent with tectonic features, and has higher resolution than, e.g., EPcrust
- Uncertainties are quantified: the model can be seen as a consensus versus model for the region

Correspondence to:

I. Molinari,
irene.molinari@erdw.ethz.ch

Citation:

Molinari, I., J. Verbeke, L. Boschi, E. Kissling, and A. Morelli (2015), Italian and Alpine three-dimensional crustal structure imaged by ambient-noise surface-wave dispersion, *Geochem. Geophys. Geosyst.*, 16, 4405–4421, doi:10.1002/2015GC006176.

Received 16 NOV 2015

Accepted 27 NOV 2015

Accepted article online 8 DEC 2015

Published online 31 DEC 2015

Italian and Alpine three-dimensional crustal structure imaged by ambient-noise surface-wave dispersion

I. Molinari¹, J. Verbeke², L. Boschi³, E. Kissling¹, and A. Morelli⁴
¹Department of Earth Sciences, Institute of Geophysics, ETH Zurich, Switzerland, ²CGG, Paris, France, ³Sorbonne Universités, UPMC Univ Paris 06, CNRS, Institut des Sciences de la Terre de Paris (iSTeP), 4 place Jussieu 75005 Paris, France, ⁴Istituto Nazionale di Geofisica e Vulcanologia, Sezione di Bologna, Italy

Abstract We derive the 3-D crustal structure (S wave velocity) underneath Italy and the Alpine region, expanding and exploiting the database of ambient noise Rayleigh-wave phase- and group-velocity of Verbeke et al. (2012). We first complement the database of Verbeke et al. (2012) with a dense set of new ambient-noise-based phase-velocity observations. We next conduct a suite of linear least squares inversion of both phase- and group-velocity data, resulting in 2-D maps of Rayleigh-wave phase and group velocity at periods between 5 and 37 s. At relatively short periods, these maps clearly reflect the surface geology of the region, e.g., low velocity zones at the Po Plain; at longer periods, deeper structures such as Moho topography under Alps and Apennines, and lower-crust anomalies are revealed. Our phase- and group-velocity models are next inverted via the Neighbourhood Algorithm to determine a set of one-dimensional shear-velocity models (one per phase/group-velocity pixel), resulting in a new three-dimensional model of shear velocity (v_s) parameterized in the same way as the European reference crustal model EPcrust. We also show how well v_s is constrained by phase and group dispersion curves. The model shows the low velocity area beneath the Po Plain and the Molasse basin; the contrast between the low-velocity crust of the Adriatic domain and the high-velocity crust of the Tyrrhenian domain is clearly seen, as well as an almost uniform crystalline crust beneath the Alpine belt. Our results are discussed from the geological/geodynamical standpoint, and compared to those of other, interdisciplinary studies.

1. Introduction

Detailed maps of the seismic structure of the crust are valuable because they reflect the effects of past and present tectonic processes, and because crustal structure must be known if seismic data are used to image deeper, mantle structure or to constrain the parameters that define seismic events. Seismic observations are very sensitive to crustal structure, but are often unable to image it unambiguously. In particular, teleseismic observations are affected by seismic velocities and depth of discontinuities within the lithosphere, in particular the Moho, but it is hard to separate crust and mantle effects by analyzing teleseismic data alone. As a consequence, seismic tomography studies often rely on a priori descriptions of crustal structure, not necessarily based on direct observation [e.g., Arlitt et al., 1999; Auer et al., 2014, and references therein]. An inaccurate crustal model may significantly reduce the accuracy of mantle imaging [e.g., Bozdag and Trampert, 2008], and our knowledge of the long-wavelength seismic structure of the crust is still, in many instances, unsatisfactory.

The Alpine and Apennines mountain ranges have been the subject of countless geological and geophysical studies for the last two centuries at least [e.g., Doglioni et al., 1999; Handy et al., 2010, and references therein]. Owing to the mentioned difficulties in crustal imaging, a number of fundamental questions are still open concerning orogeny and mantle dynamics in this complex area [Faccenna and Becker, 2010]. Local-scale crustal models have been derived from geological data sets [Molinari et al., 2015], active reflection and refraction seismic experiments [e.g., Waldhauser et al., 1998; Brückl et al., 2007], P-wave travel-time tomography [e.g., Chiarabba and Amato, 1996; Piromallo and Morelli, 2003; Serretti and Morelli, 2011; Gualtieri et al., 2014], local earthquake tomography (LET) [e.g., Diehl et al., 2009; Di Stefano et al., 2009], receiver-function studies [e.g., Piana Agostinetti and Amato, 2009], and combinations of the latter two data types [Wagner

et al., 2012; *Spada et al.*, 2013]. These methods provide important constraints on three-dimensional (3-D) P-wave velocity structure and on the depth of sharp discontinuities. However, they all have intrinsic limitations: the scarcity of seismic events in large regions prevents LET to be applied at a regional scale; observations of receiver functions are limited to station locations and thus relatively sparse; active seismic experiments need 3-D migration [*Waldhauser et al.*, 1998]. Hence, these techniques cannot be easily applied at large scales. Even more importantly, none of them constrains S-wave velocity (v_s) directly. Some studies have combined information from different methods, to determine larger-scale crustal models [e.g., *Tesaura et al.*, 2008; *Grad et al.*, 2009; *Baranov*, 2010; *Molinari and Morelli*, 2011; *Molinari et al.*, 2012]. This approach requires some subjective assumptions: for instance, information from distantly neighbouring refraction profiles could be interpolated on the base for instance of gravity data, and v_s could be derived by scaling P-wave velocity (v_p) using some standard relations. Crustal v_s -sensitive data are much sparser than v_p -sensitive ones, and current crustal models of v_s are relatively unreliable.

The recent introduction of seismic interferometry has allowed to map crustal v_s by observing surface waves in seismic ambient noise [e.g. *Shapiro et al.*, 2005; *Boschi and Weemstra*, 2015, and references therein]. As a general rule, surface waves are much more sensitive to v_s than to v_p . While teleseismic surface-wave observations are limited to long periods and thus mostly affected by mantle structure [e.g., *Boschi and Ekström*, 2002], ambient-noise seismology allows to measure surface-wave dispersion at shorter “epicentral” distances, and at shorter periods: in practice, this means that ambient-noise surface-wave data are sensitive to crustal and lithosphere structure but not to the mantle. Today, a number of authors apply ambient-noise interferometry to reconstruct the structure of the crust with increasing resolution, in regions covered by networks of seismographic stations. For instance, *Delorey and Vidale* [2011] have been able to refine a 3-D v_s model of the Seattle area for seismic hazard assessment purposes; *Zulfakriza et al.* [2014] retrieved the upper crustal structure of central Java (Indonesia) from transdimensional seismic noise tomography; *Saygin and Kennett* [2012] imaged the Australian crust; *Kao et al.* [2013] imaged the crust and upper mantle v_s structure of Canada and adjacent regions; *Lin et al.* [2008] and *Ekström* [2014] have studied North American crustal structure via phase- and group-velocity maps; preliminary ambient-noise studies of Alpine crustal structure have been conducted by *Stehly et al.* [2009], *Fry et al.* [2010] and *Li et al.*, [2010].

Verbeke et al. [2012] compiled a large database of surface-wave dispersion measurements from seismic ambient noise in the Alpine and Italian regions. Their group-velocity maps at periods between 5 and 40 s reveal velocity anomalies with high detail, not exploited yet to define a 3-D crustal model. These data have strong sensitivity to crustal v_s structure, but weak sensitivity to discontinuities and their depth. The geometry of crustal seismic discontinuities under Italy and the Alps, however, has been determined in a number of studies using other observation techniques: model EPcrust [*Molinari and Morelli*, 2011] includes robust interface geometry determinations based on seismic reflection and refraction studies; *Spada et al.* [2013] have constrained Moho depth via controlled-source seismology, local earthquake tomography and receiver-function analysis; the 3-D structure and depth of the deep Po-plain sedimentary basin has been determined from geological data [*Molinari et al.*, 2015].

In this study, we derived the 3-D crustal structure (S wave velocity) underneath Italy and the Alpine region, expanding and exploiting the database of *Verbeke et al.* [2012]. We first derive new maps of fundamental-mode Rayleigh-wave group- and phase-velocity, making use of phase-velocity observations that were not available to *Verbeke et al.* [2012], and enhancing lateral resolution significantly. The study of *Verbeke et al.* [2012] was limited to phase- and group-velocity maps; here we infer 3-D v_s structure using a fully nonlinear direct-search inversion algorithm [*Wathelet*, 2008]. This method allows for a priori information other than seismic dispersion curves to be taken into account in the inversion: we thus combine ambient-noise surface-wave data with the above-mentioned, independent observations of discontinuity depths, which surface waves are only weakly sensitive to; in practice, the resulting 3-D map can be seen as a model integrating information on receiver functions and surface wave.

In the following, we first describe the linear tomographic inversion that provides phase- and group-velocity maps; we next illustrate the results of the nonlinear inversion for v_s , including an assessment of uncertainties; finally, we discuss our results from the geological/geodynamical standpoint, and compare them to those of other, interdisciplinary studies.

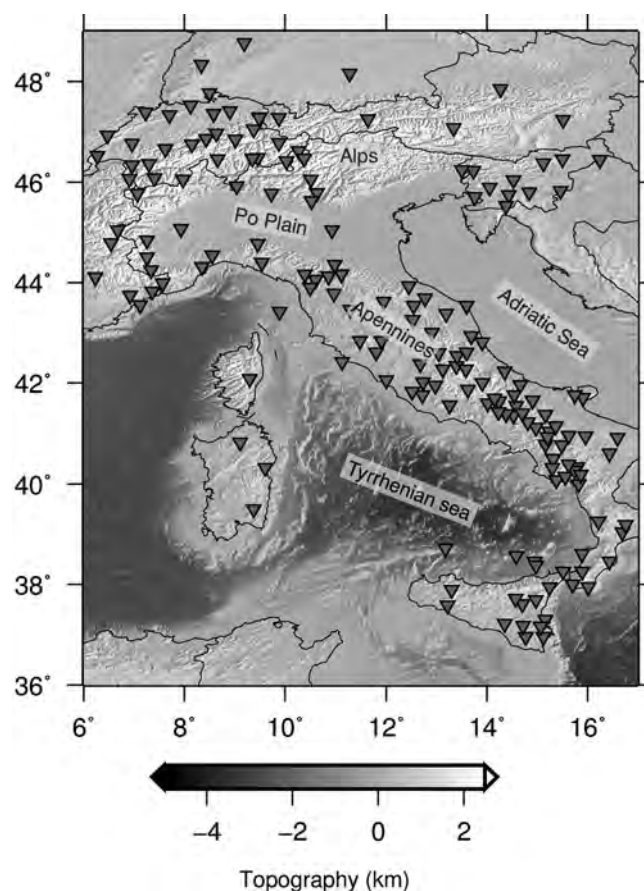


Figure 1. Stations where the ambient noise analyzed in this study was recorded.

2. Rayleigh-Wave Phase Velocity Maps From Ambient Noise

Verbeke *et al.* [2012] have built a database of Rayleigh wave group and phase velocity measurements from seismic ambient noise extending across Italy and the Alps toward Central Europe. Following Bensen *et al.* [2007], they cross-correlated and analyzed 1 year (2008) of continuous vertical-component seismograms recorded by pairs of stations belonging to the Italian, Swiss and German permanent broadband networks (Figure 1). For each station pair, surface-wave group velocities have been measured applying the time frequency analysis (FTAN) method [Ritzwoller and Levshin, 1998], while phase velocities have been obtained following the two-station method as implemented by Meier *et al.* [2004]. The accuracy of phase-velocity measurements was verified by Boschi *et al.* [2013], who validated the method used by Verbeke *et al.* [2012] against an independent approach based on frequency-domain cross-correlation.

Our database is based on that of Verbeke *et al.* [2012]. With respect to the work of Verbeke *et al.* [2012], group-velocity data are exactly the same, while phase-velocity dispersion curves have been entirely recomputed from the original cross-correlations, to include phase-velocity measurements made at a denser and broader set of frequencies as illustrated in the following. With respect to group velocity, phase-velocity data sample a wider depth range and are less contaminated by interfering phases, because measurements are made within a narrower time window [e.g., Boschi *et al.*, 2013]. On the other hand, group velocities are more sensitive to relatively shallow depth and are easier to measure. We take advantage of both data types to constrain 3-D crustal structure at the highest possible resolution. After measuring dispersion as described between all available station pairs (Figure 1), we derive phase-velocity maps between 5 and 37 s periods and group-velocity maps from 8 to 35 s.

2.1. Phase- and Group-Velocity Imaging Method

Assuming, as is done in most seismic ambient-noise literature, that the effects of nonuniformity in noise source distribution can be neglected, an ambient-noise database is equivalent to a “traditional” one, with earthquake sources replaced by seismic stations acting as “virtual” sources [Boschi and Weemstra, 2015]. We set up a linear system in the ray-theory approximation as described, e.g., by Boschi and Dziewonski [1999]. Based on the available ray coverage, we parameterize the region of interest in terms of $0.25^\circ \times 0.25^\circ$ cells, independent of period and for both phase- and group-velocity. We take the phase- and group-velocities predicted by PREM [Dziewonski and Anderson, 1981], period-dependent but laterally homogeneous, as reference values, and determine phase- and group-velocities through a suite of least-squares inversions (one per period for both group and phase data) via the iterative LSQR algorithm [Paige and Saunders, 1982]. LSQR approximates the exact least square solution, converging, according to a rigorous “stopping criterion” [Paige and Saunders, 1982], after some tens of iterations. In order to obtain a stable solution, we regularize the inverse problem via the roughness minimization scheme of Boschi and Dziewonski [1999], which is

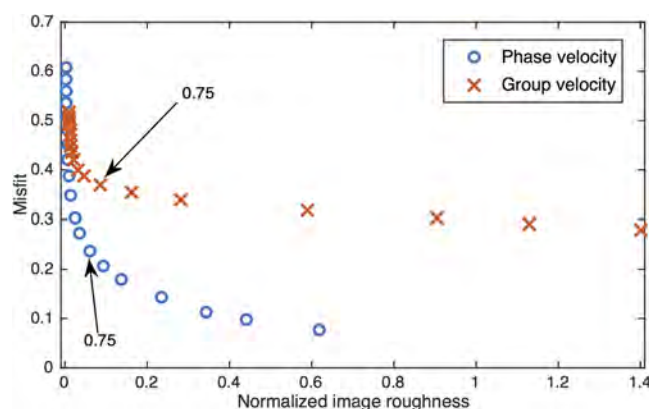


Figure 2. L-curve resulting from phase (red crosses) and group (blue circle) inversions for 16 s period. Selected models are marked by arrows and labeled by the corresponding value of the roughness-damping parameter [e.g., *Boschi and Dziewonski, 1999*]. The image roughness is defined as the squared modulus of the dot-product of roughness damping matrix times vector of model coefficients. It is normalized dividing by the total sum of squared model coefficients. Following e.g., *Boschi [2006]*, we show here misfit defined as one minus variance reduction.

in Figure 2: the roughness damping value is 0.75 for both phase and group velocity and for all periods. As can be expected, variance reduction changes as a function of surface-wave period. Highest variance reductions (up to $\sim 75\%$) of both group and phase data are achieved in the 8–25 s period range; at periods < 8 s and > 25 s variance reduction does not exceed 50%.

2.2. Resolution Test

We quantify the horizontal resolution of phase- and group-velocity allowed by our dispersion data sets via synthetic tests [e.g., *Boschi and Dziewonski, 1999*]. Following *Husen et al. [2009]* and *Verbeke et al. [2012]*, we choose as “input” model a random 2-D map of velocity anomalies (Figure 3) whose size and distribution is statistically similar to typical seismic maps at this scale length. This is preferable to unrealistic though widely used “checkerboard” input models who tend to yield too optimistic estimates.

The input model of Figure 3 is characterized by anomaly values ranging between -10% and $+10\%$ with respect to PREM [*Dziewonski and Anderson, 1981*], filtered via 2-D Fourier transformation to isolate the wavelengths of interest, resulting in anomalies of spatial extension > 50 km and < 200 km. We calculate phase and group delay times predicted by this model for all ray paths and periods in our database (station coverage depends on period and on whether phase or group velocity is measured); we add Gaussian noise to the data (the standard deviation of random noise is the same as that of the data, $\sigma = 0.2$ km/s). Finally, we solve the two inverse problems—for phase and group velocities—using the inversion algorithm and regularization scheme and parameters that we apply to our real data set. The results associated with 7, 12 and 20 s Rayleigh-wave phase velocity data and with 8, 16, 24 s group velocity data are shown in Figure 3. We only show our solution in cells sampled by more than 5 rays, estimating that less well sampled pixels might not be sufficiently well constrained. As a general rule, the test model is recovered fairly well, within the resolved area, independently of period; group velocity, for which we have a denser ray coverage (see maps in Figure 3), is recovered more accurately than phase velocity; amplitude of both phase- and group-velocity anomalies is underestimated. At short periods (up to 14 s), phase velocity is resolved well in Switzerland, Southern Germany, Western and Eastern Alps and North-Western Apennines; at longer periods phase-velocity resolution becomes acceptable also in North-Eastern, Central and Southern Italy. Group-velocity resolution is fairly good throughout the region of interest, with the exception of Western Tyrrhenian Sea, Sardinia, Corsica and Southern Adriatic sea.

We anticipate that, as a consequence, the resolution of our final 3-D model changes as a function of location (and not only in depth, due to differences of depth sensitivity for phase and group velocity at each period, see section 2.3): in areas where short period surface-wave velocity is not constrained by either group or phase dispersion observation, shallow crustal structure is underconstrained (see section 3.2).

equivalent to requiring the solution model to be smooth. We do not apply norm minimization because, in cases of nonuniform data coverage, this form of regularization can result in solution models with unnaturally large velocity gradients [e.g., *Boschi and Dziewonski, 1999*]. We carry out many tentative inversions with different regularization parameter values until a satisfactory solution is achieved, i.e., (i) variance reduction of the data is relatively high; (ii) using resolution tests (sec. 2.2) as a reference, we verify that there are practically no features in our maps at wavelengths shorter than our target resolution. We verified that solutions found in this way correspond to the corner region of the L-curve as defined by *Hansen [1992]* and shown

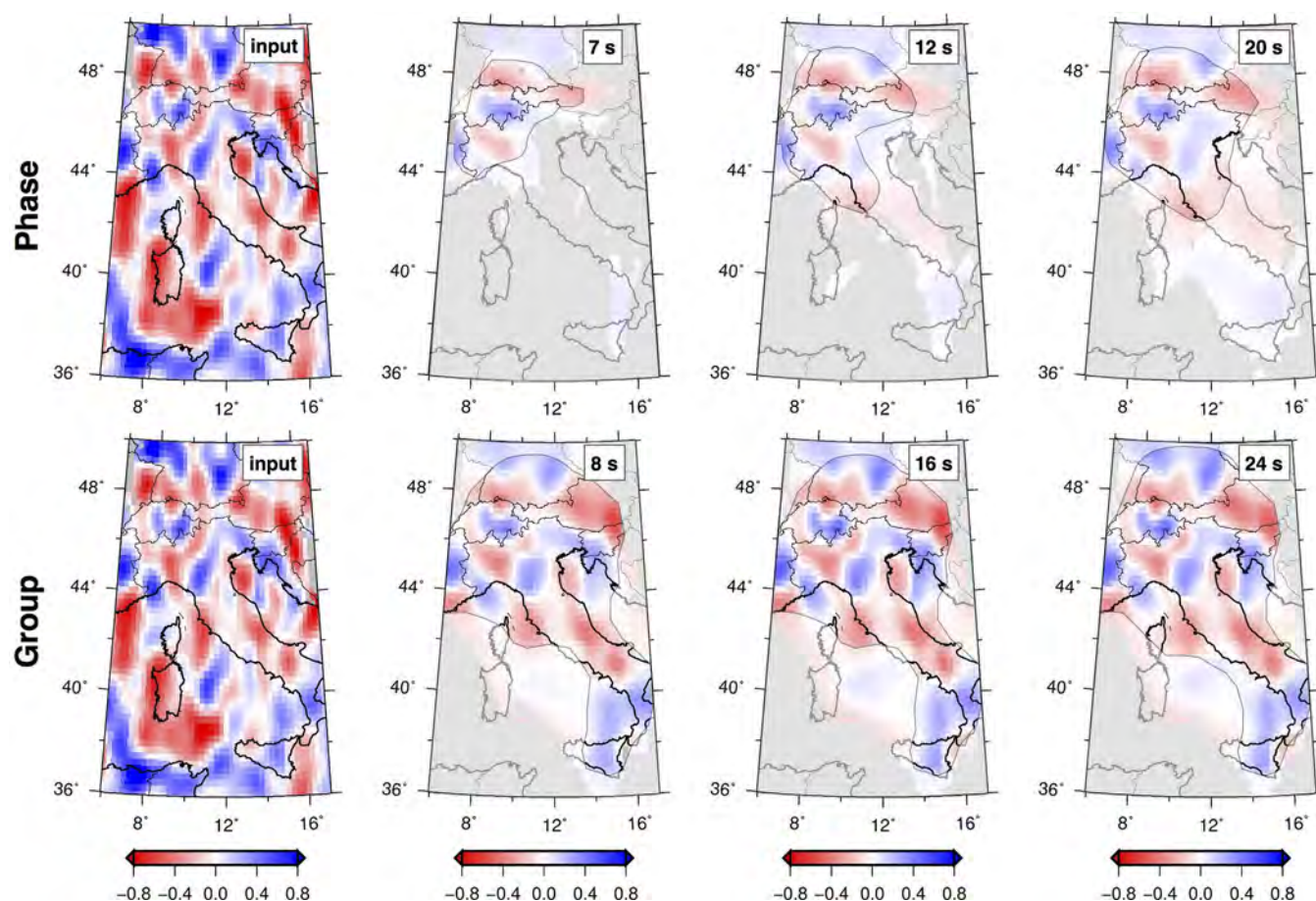


Figure 3. Results of the reconstruction test with randomly distributed velocity anomalies as input. The left plots show the input models used while the other columns show retrieved models at different periods as indicated for phase (top row) and group (bottom row) velocity. We highlight the well resolved area with the grey line for each shown period.

2.3. Rayleigh-Wave Phase- and Group-Velocity Maps

We show in Figure 4 the phase and group velocity maps obtained from our data sets at periods between 5 s and 37 s, and 8 s and 35 s, respectively. Long-period surface waves sample deeper into the Earth and are correspondingly characterized by higher velocities than short-period ones, as noted in Figure 4. As a first order approximation, surface waves of 7 s image structure from surface down to 10 km depth, those of 20 s period are most sensitive to structure between 10 km and 30 km, and those of 37 s period between 35 km and 55 km depth [Warren *et al.*, 2013]. At any given period, group velocity is sensitive to structure at shallower depth than phase velocity.

The longer wavelength patterns of the maps in Figure 4 are in agreement with the lower-resolution maps of Verbeke *et al.* [2012]. At short periods we clearly recognize the effects of shallower geological features. Low-velocity anomalies (~ 2.3 km/s for phase and < 1.5 km/s for group velocity) can be associated to sedimentary basins in the Po plain, known to be characterized by a low seismic velocity foredeep sedimentary basin that reaches a depth of 7–8 km and to a lesser degree in the Swiss and German Molasse basin (visible especially well in the 8 s group velocity map). As expected for shallow crustal levels, the Alpine belt exhibits higher velocities than the Apennines, indicating the presence of shallow high-velocity crystalline structure in the Alps.

At intermediate periods (12 s for phase and 16 s for group velocity) the signature of the Po Plain is still clearly visible, suggesting that deep and slow sedimentary basins affect the dispersion curves at longer periods more than estimated by theoretical maximum sensitivity. This means that, in order to get a realistic velocity 3-D model in this region, we need to constrain those basins with a good a priori model. Using a finer parameterization grid, we recover the Ivrea body high-velocity zone at lon $\sim 8^\circ$ and lat $\sim 44.5^\circ$ (Figure 3).

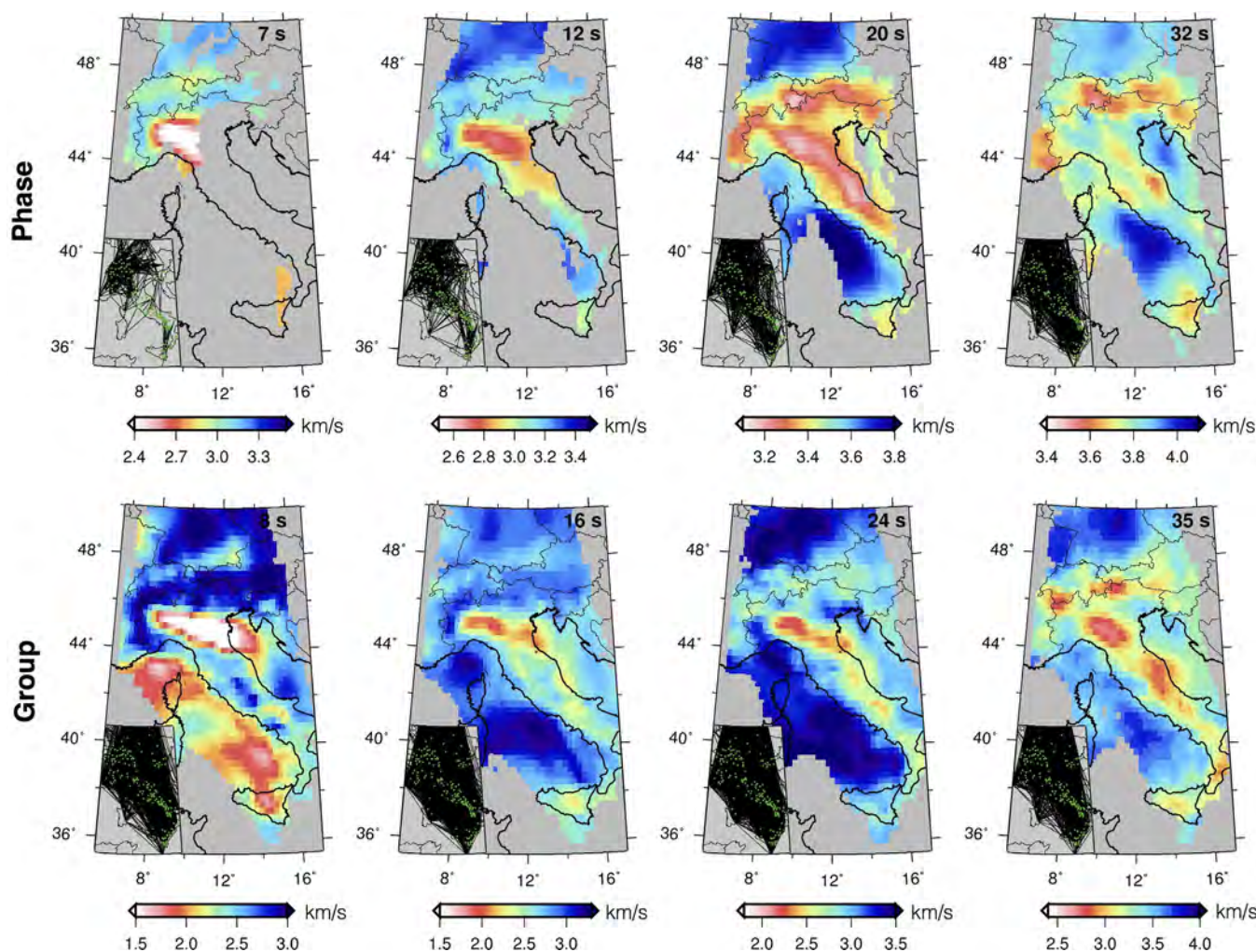


Figure 4. Maps of (top) phase velocity and (bottom) group velocity resulting from tomographic inversion of ambient-noise dispersion data. Period (s) is specified on each map, and grows from left to right. The shortest periods are sensitive e.g., to the thickness of the sediment layer, while the longest ones sample the crust down to depths close to that of the Moho and below [e.g., Fry *et al.*, 2010, Figure 5]. We also show the ray coverage for each period (insets).

Lower phase and group velocities are found along the Apennines than along the Alps, presumably owing to the different properties of rocks forming the uppermost part of the crust under those two mountain ranges: the Apennines are predominantly characterized by Adriatic consolidated sediments with a low degree of metamorphism, as opposed to relatively high-velocity crystalline upper-crustal and metamorphic basement rocks under the Alps. High velocities appear mainly over the Tyrrhenian Sea, as a result of the shallow Moho depth in this oceanic region.

Longer periods (20 s and 32 s for phase; 24 s and 35 s for group velocity) are most sensitive to lateral variations of lower crust, Moho depth and uppermost mantle, depending on location. The contrast between Tyrrhenian and Adriatic crust is strong (about 0.3–0.4 km/s), but this effect is explained to a large extent in terms of Moho depth, the Tyrrhenian crust being anomalously thin with respect to the rest of the region of interest. At periods > 30 s, we can clearly distinguish the deep crustal root along the inner parts of the Alpine orogen and beneath the Apennines, and the low-velocity anomaly proposed by Di Stefano *et al.* [2009] as the “Central Apennine” window, based on P-wave travel-time tomography.

3. Inversion for 3-D Structure

At each cell of our phase-/group-velocity maps, we construct fundamental-mode Rayleigh-wave dispersion curves, ranging from 5 to 37 s period in phase velocity, and 8 to 35 s in group. We subsequently invert each

Table 1. Setting of the Variability Range of the Parameters in the Inversion With Respect to the a Priori Informations^a

	Thickness	v_s (km/s)	v_p (km/s)	Density (g/cm ³)
Top layer – sedimentary basins	± 5%	1.2–3.4	3.3–5.5	2.4
Top layer – others	1–5 km	2.5–3.6	5.7–6.8	2.7
Upper crystalline crust	± 10%	2.8–3.7	6.2–7.0	2.75
Lower crust	± 10%	3.1–4.0	6.8–7.5	2.9
First mantle layer	fixed	± 10%	fixed	fixed
Second mantle layer	fixed	± 6%	fixed	fixed

^aMAMBo model [Molinari *et al.*, 2015] in the Po basin, EPcrust velocity range in the crust and EPmantle in the mantle.

combination of phase- and group-velocity dispersion curves, to determine isotropic v_s , v_p and layer thicknesses. Each inversion consists of a stochastic direct search, implemented via the “Neighbourhood Algorithm” [Sambridge, 1999a; Wathelet, 2008]. In this approach, the solution space is sampled sequentially and nonuniformly, taking into account the data fit achieved by old samples when generating new ones: in practice, while possible solutions are sought randomly, the search is biased toward regions of the solution space where better-fitting solutions have been found [Wathelet, 2008]. The cost function is the L2-norm of the difference between the observed dispersion curves, and those calculated from a solution model.

This approach is suited to the inverse problem under consideration because of its inherent nonlinearity. It has the advantage of widely exploring the admissible solution space, without anchoring the solution model to the reference one as would happen in a linearized inversion. However, the strong nonlinearity of the problem and the averaging properties of the dispersion measurements can always result in significantly biased solutions, especially in combination with deep sedimentary basins or wherever particularly strong velocity discontinuities are present. Naturally, where data coverage is poor, nonlinear inversion can result in strong depth variations clearly incompatible with known geological features [Saygin and Kennett, 2012]. As mentioned above, the main weakness of surface-wave inversion is the lack of sensitivity to the depth of seismic interfaces. Following Wathelet [2008], we therefore define the boundaries of the solution space to be sampled (i.e., the range of possible values for all parameters we invert for), on the basis of a priori information from independent geophysical and geological data. A priori constraints on the model search are important to speed up the inversion by limiting the volume of model space searched and to define what we judge to be physically plausible candidate models.

The vertical parametrization of our 3-D models is the same as that of EPcrust, including three crustal layers plus two 25 km thick mantle layers. The three crustal layers are defined as the following: a top layer which can be either sediment in the sedimentary basins (Po Plain, Molasse basin and Ligurian Sea basin), a stack of sedimentary thrust sheets in i.e., Apennines or upper-most crustal like material; a middle layer corresponding to the crystalline upper crust; a lower layer corresponding to the lower crust. v_s in each layer is described with a linear gradient, obtained by subdividing each layer into five sublayers. The water layer is not taken into account: this simplification, inherent limit of our inversion software, might cause biased results under Tyrrhenian Sea. Since our study is focused on continental structure, we think it is reasonable to “neglect” this layer for the time being. The allowed parameter ranges in each layer are defined based on the most recent crustal models and Moho maps of the region of interest. Upper- and lower-crustal parameters (especially v_p and density) should be in the same range as EPcrust values; velocities in the mantle should be similar to EPmantle values [Schivardi and Morelli, 2011]; Moho depths are required to be close to those given by Spada *et al.* [2013]; in the Po Plain, sediment-layer thickness and velocity should resemble those provided by the MAMBo model [Molinari *et al.*, 2015]. Outside the Po Plain, we allow the top-layer thickness to vary between 1 and 5 km. The exact variability range of each parameter is given in Table 1.

Each inversion consists of a nested exploration of the solution space, carried out in 140 steps; at each step, the 110 best-fitting solutions are kept. In summary, 35,400 possible solution models are evaluated at each cell. In Figure 5, the best-fitting 15,400 models are plotted for a few sample cells, illustrating the range of possible models sampled by the inversion, and the goodness of fit they achieve. The similarity between best and mean models in Figure 5 reflects the velocity resolution afforded by our database: the solution is generally robust (similar to the mean) except for the first few kilometers, and for the top of the mantle.

We run our algorithm once for each of the $0.25^\circ \times 0.25^\circ$ pixels of our dispersion maps. The root mean square (RMS) of the misfit is shown, as a function of period, in Figure 6, where we compare the fit achieved by

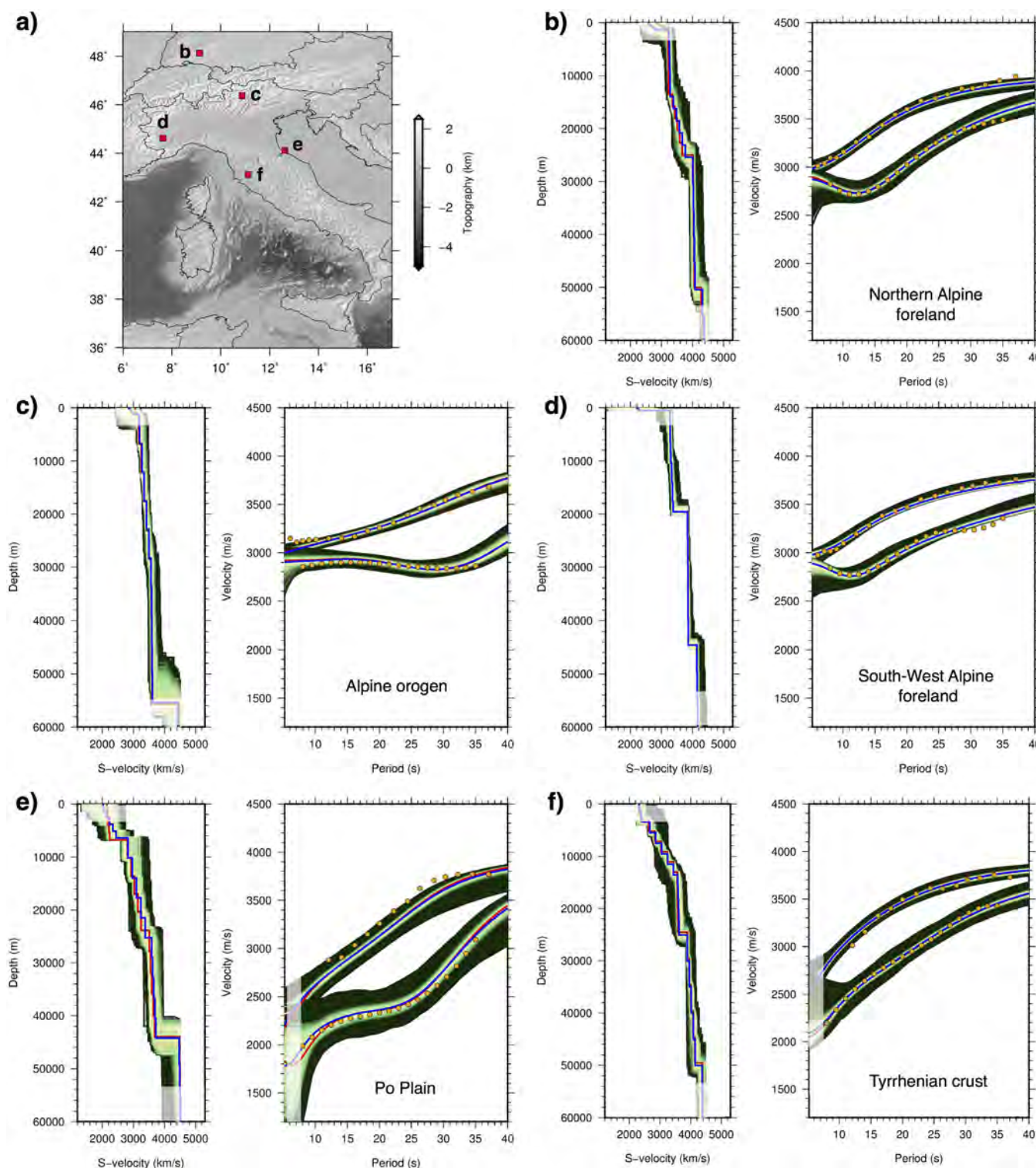


Figure 5. 1-D profiles of the v_s resulting from inversion. Parameterization is the same as EPCrust (i.e., three crustal layers, and two mantle layers). The panels refer to a different sample cell shown in (a) Northern Alpine, (b) Foreland, (c) Alpine Orogen crust, (d) South-West Alpine foreland, (e) Po Plain, and (f) Tyrrhenian crust. In each main plot, the suite of resulting v_s profiles, as a function of depth, and corresponding Rayleigh phase and group dispersion curves, as a function of period, are shown. Both types of curves are plotted with different colour depending on data misfit (colour scales vary slightly). The red line represents the best model, while the blue line represents the preferred model (average of the best 500 models) in both depth profiles and dispersion curves plots. We reduce the colour intensity in all regions where we have no observations (i.e., periods shorter than 5 s and at depth above the 5–6 km and below the 50 km).

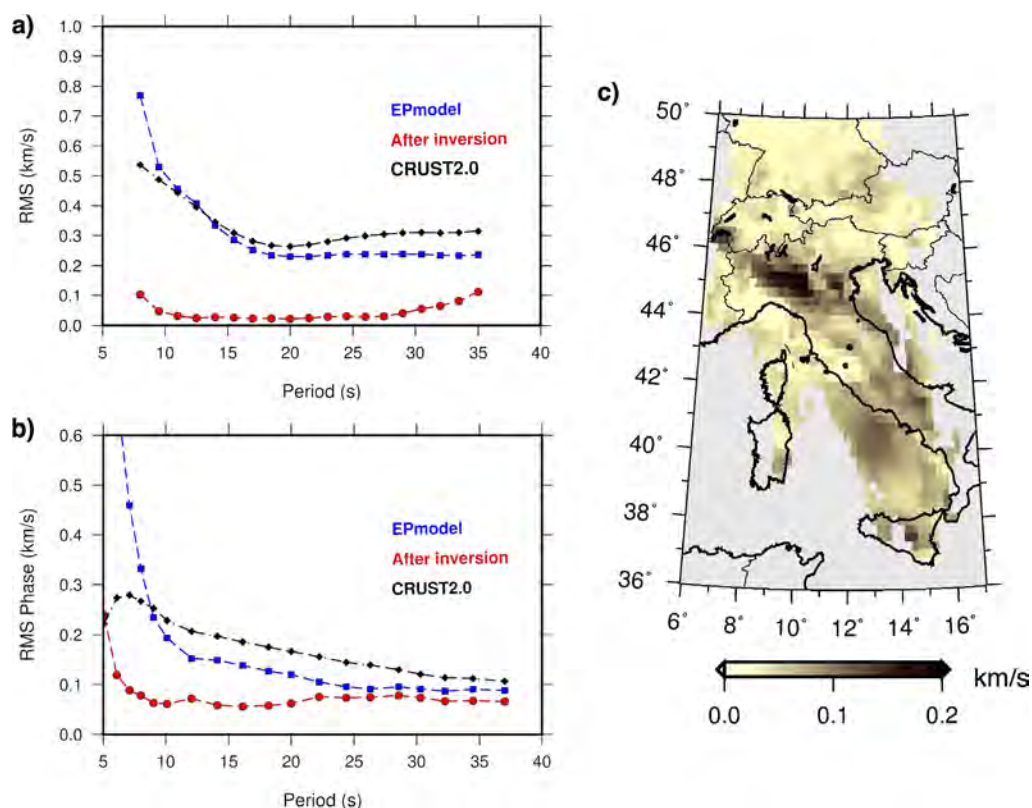


Figure 6. The root mean square (RMS) in km/s of the misfit to ambient-noise-based (a) group and (b) phase velocity at various periods over all the cells, achieved by EPcrust (squares), by CRUST2.0 (diamonds) and by the model we obtain after 3-D inversion (circles). (c) Map of the RMS in each cell for group and phase velocity together.

crustal models EPcrust and CRUST2.0 [Bassin *et al.*, 2000] and by our final best model. We infer from Figure 6 that inversion improves data fit significantly with respect to existing regional models. The improvement of fit is particularly remarkable at periods < 15 s, where both EPcrust and CRUST2.0 show large deviations from measured data. This could be ascribed to inaccurate EPcrust/CRUST2.0 estimates of uppermost crustal layer, at least in some regions. Importantly, EPcrust and CRUST2.0 (i) are continental-/global-scale models, not designed to be employed at the scale of this study, and (ii) they were derived from observations independent of surface waves (whether earthquake or noise-generated). The fact that EPcrust and CRUST2.0 reduce the variance of our ambient-noise data at most periods is a nontrivial result, and a significant validation of those models.

Figure 6c shows the geographical distribution of model misfit. The misfit is highest at sedimentary basins and at North-West border of our region of interest. The overall misfit strongly depends on whether a good fit is achieved at the shortest periods, where poor estimates of top crustal layer thickness and velocity and coarse parameterization can easily deteriorate it, and at the longest periods in consideration, where ambient-noise-based measurements are scarcer.

Our final best-fitting model ultimately accounts for a broad variety of data; it strongly improves the fit of surface-wave dispersion observations and additionally accounts for a-priori knowledge of crustal structure derived by other independent methods; it is overall an important upgrade of EPcrust, in particular as far as v_s structure is concerned.

3.1. Local Velocity Profiles

In Figure 5, we select examples of nonlinear v_s inversions involving a diverse set of geological settings. Our group- and phase-velocity data, combined with the mentioned a priori information on the depth of the main sedimentary basins and, in particular, of the Moho depth, allow us to map v_s crustal structure with higher resolution than previously possible. The lack or poor quality of data at very short periods (< 5 s) may

lead to near-surface velocities that are poorly correlated with geology, but this effect is marginal, owing in particular to the careful a-priori constraint introduced in our inversion strategy as explained above.

We noted that both phase- and group-velocity data are generally well explained by our model. In areas where crustal structure is particularly complex (e.g., deep sedimentary basins, Moho offsets at plate boundaries), the data fit is occasionally poor: the problem might be solved by means of a local, ad-hoc, finer parameterization, but this would be extremely time-consuming and is beyond the scope of this study.

Figure 5b corresponds to the Northern border of the Molasses basin, and is representative of European lithosphere outside the orogenic belts. We find here a crustal thickness of about 25 km, with an almost uniform upper crust and a large velocity gradient in the lower crust. The Moho appears to be relatively shallow, but a closer look at Figure 5b shows that many solution models exist that fit the data about equally well.

In the Alpine orogen cell (Figure 5c) our model is characterized by a relatively high near-surface velocity of about 3.15 km/s reflecting the granitic basement rocks exposed at surface after intensive uplift and erosion. The Moho is more than 50 km-deep [Schmid and Kissling, 2000], near the lower limit of resolution by our data. That the Moho is anomalously deep could be directly inferred from the phase-velocity dispersion curve, where the kink typically associated to Moho depth [Lebedev *et al.*, 2013] is not found, presumably because it takes place at longer periods, outside our measurement range.

The south-west Alpine foreland cell (Figure 5d) is located at the Southern edge of the Ivrea Body [Solarino *et al.*, 1997], and shows very low surface velocity of about 2.3 km/s and velocities of about 3.4 km/s in the whole crust, in good agreement with known near-surface structure. Imaged Moho depth is relatively shallow (20 km), corresponding to the Ivrea mantle upwelling [Spada *et al.*, 2013].

In the Po Plain, along the Adriatic coast (Figure 5e), Tertiary and Mesozoic sediments reach 7 km thickness [Molinari *et al.*, 2015]. Their effect is visible in the corresponding dispersion curves up to 25–30 s period; group velocity is particularly low, i.e., ~ 2 km/s at period < 15 s. We emphasize that, in this anomalous location, our a priori definition of the solution space plays a particularly important role: we have only explored solution models that included a thick sediment layer. Preliminary inversions had shown that, in the absence of such constraint, group- and phase-velocity anomalies would have been explained in terms of very low v_s throughout the crust. Despite that, a broad range of plausible solution models are shown in Figure 5e, suggesting that this remains a relatively poorly constrained location that could benefit from further seismic observations of all kinds. Besides the thick sediment layer, our best profile at this location includes upper crustal basement rocks of cumulative thickness > 15 km, overlying rather average Adriatic lower crust.

The last cell is representative of the Tyrrhenian crust (Figure 5f). At this location the Moho is relatively deep (~ 25 km); the upper crust is characterized by a strong velocity gradient; the middle-lower crust is approximately uniform.

3.2. Model Variability

Before discussing 3-D v_s variations, we evaluate how robustly they are constrained by our procedure. Non-linear, direct-search inversion techniques — such as the Neighbourhood Algorithm used here — allow the exploration of the model space, guided by explicit a priori informations that designate physically plausible models on the basis of supplementary data. This approach can thus provide an assessment of the range of “possible” models — i.e., those that reach an acceptable fit to observations — in a more general fashion than linearized standard error analyses. While a rigorous model appraisal, geared for accurately picturing posterior probability density functions in a Bayesian sense, may often be an expensive task [Sambridge, 1999b], the suite of models tested during the search stage provides a fair picture of model uncertainty. Our nonlinear search technique [Sambridge, 1999a; Wathelet, 2008] generates an ensemble of acceptable models that may be taken to represent the posterior probability distribution function (PDF) of the earth structure reflected by the observations. We limit our estimation of model variability to this approximate PDF representation.

The marginal velocity probability density distribution of a single model parameter (i.e., shear-wave velocity at some particular depth in vertical v_s profile) appears well behaved, not far from a Gaussian. This can be verified in Figure 7, that shows the distribution of v_s values at three fixed depths for a sample geographical location (cell e) in Figure 5). The a priori PDFs — in each case, a boxcar representing a range of variability with uniform probability density — is also plotted, showing that significant improvement in information is

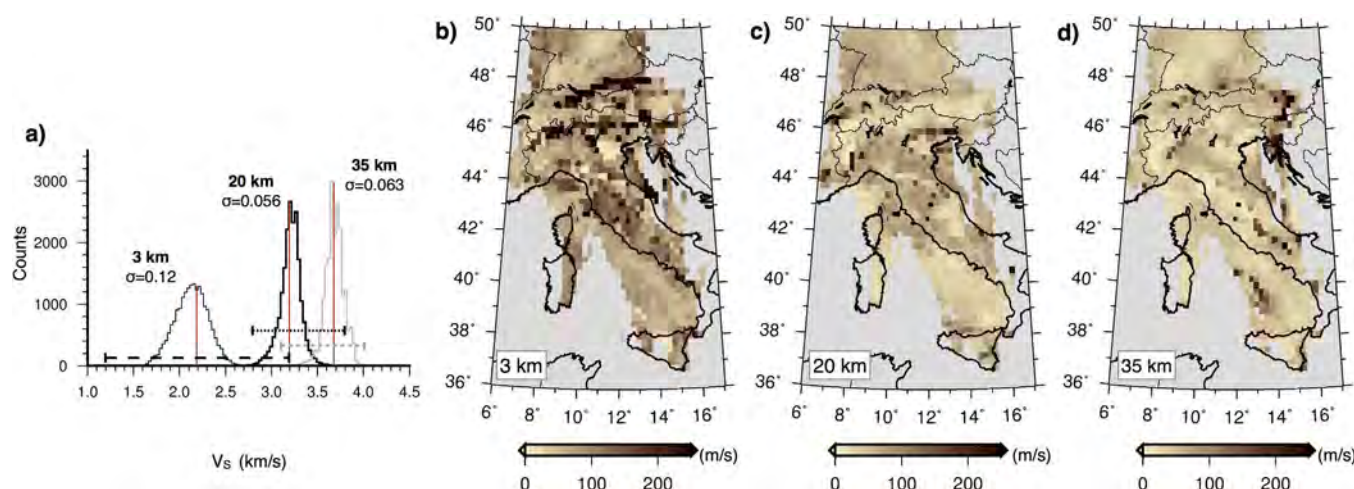


Figure 7. (a) Variability range for the v_s parameter at three different arbitrarily chosen depths representative of the three layers for the cell in Figure 5e, defined as the standard deviation of the gaussian distribution. The red lines represent the best value and the dashed lines (black and grey) the a priori range of variability allowed during the inversion for that layer. Map of the sigma calculated in each cell at (b) 3 km, (c) 20 km, and (d) 35 km depth.

reached by the inversion. Note that we sample wider velocity ranges at shallower depths, consistently with physical expectations of heterogeneity. Posterior marginal PDFs taper off near the ends of the sampled ranges, indicating that they are wide enough and compatible with information contained in the data. We may claim that the a priori distributions, being flat and noninformative, do not influence results, or the shapes of posterior PDFs. As posterior PDFs resemble Gaussians (Figure 7a), the standard deviation σ is a convenient way to represent their width, hence uncertainty [Shapiro *et al.*, 2002]. Therefore, in Figures 7b–7d, we plot maps of the standard deviation at three sample depths. We note that standard deviation is generally rather small, typically less than, say, 150 m/s, and only seldom exceed 200 m/s. Larger values of σ can be due to weak data constraints, and this is the case of dark pixels in the eastern Po Plain region. Complex crustal structure in the deep Po Plain sedimentary basin may also be a cause of larger spread of velocity values of well fitting models. Yet another case of larger indetermination may occur when the interface between two layers is placed near some specific depth, and the model v_s jumps from values of one layer to those of the next one. These maps picture the uncertainty associated to our best solution, in the inversion of shear-wave velocity profiles to fit local Rayleigh phase and group dispersion curves. We recall that the quality of fit of the dispersion maps to observed data is depicted by Figure 6 showing the geographical variation of global RMS misfit.

3.3. S-Wave Velocity Structure

The maps of v_s anomalies associated with our best-fitting model are shown in Figure 8. At each depth, the solution model is only shown in cells that are sampled by at least 5 ray paths for which both phase and group velocity measurements have been successfully obtained at 16 s period. We conservatively estimate that less well sampled cells are not sufficiently robustly constrained. The well resolved cells at each depth depends on the surface wave velocity coverage (Figure 3), at periods whose sensitivity is maximum at that depth [Warren *et al.*, 2013, Figure 7b]. As discussed in the previous section, we do not have sufficient resolution to resolve the structure of shallow sedimentary layers, which are therefore controlled, in our inversions, by a priori constraints provided by geological models.

The 3 km deep section in Figure 8 shows the uppermost part of the crust including the sediment layer. The Po basin and the Ligurian-Sea basin are the most prominent features of this image. The a-priori v_s variability range is from 1.2 to 3.2 km/s and the inversion results show a $v_s \approx 2$ km/s, in good agreement with Molinari *et al.* [2015]. The deeper part of the Molasse basin is also well marked and shows a higher velocity (2.5 km/s) than Po basin highlighting the different evolution of the two Alpine foreland basins. The Alps and Apennines shallow velocities appear to be consistent with the current surface geology knowledge: high v_s in the Alps indicating the presence of crystalline and metamorphic rocks and consolidated sediment. The Tyrrhenian back-arc basins, that has started forming in the late Miocene, is partially imaged by our tomography and shows v_s around 2.4 km/s.

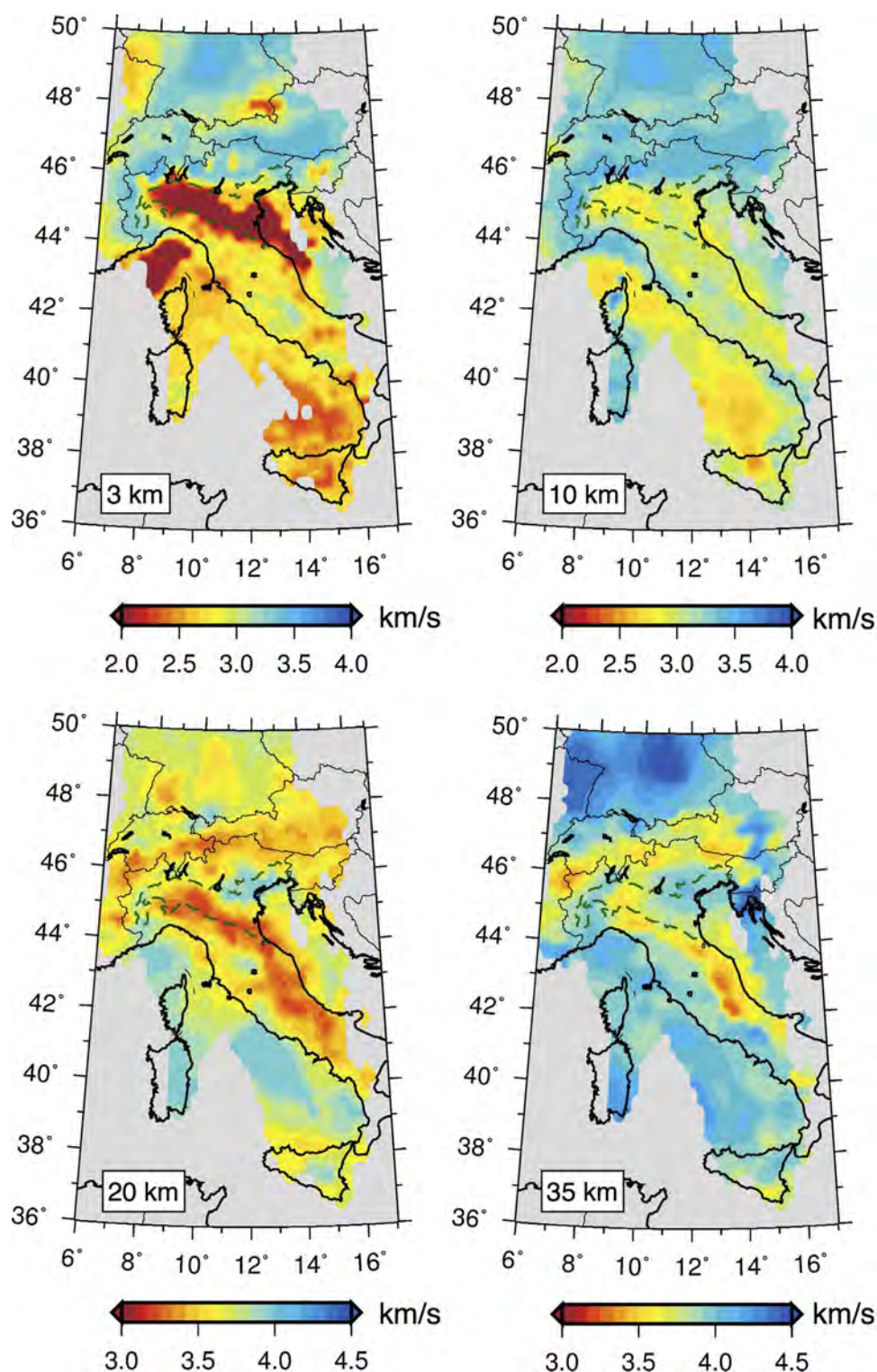


Figure 8. Maps of the shear velocity model obtained by averaging the 500 models that best-fit the data in the local neighborhood algorithm inversions. Depth in km is specified on each panel and grows left to right, top to bottom.

The 10 km deep section in Figure 8 shows a strong variability in the upper crust: distinct difference between the Alps and its Northern foreland with a uniform v_s of about 3.2 km/s while South of Alps a the same depth we find the various lithologies from the deep Po Basin sediments ($v_s \approx 2.8$ km/s) to uppermost crystalline

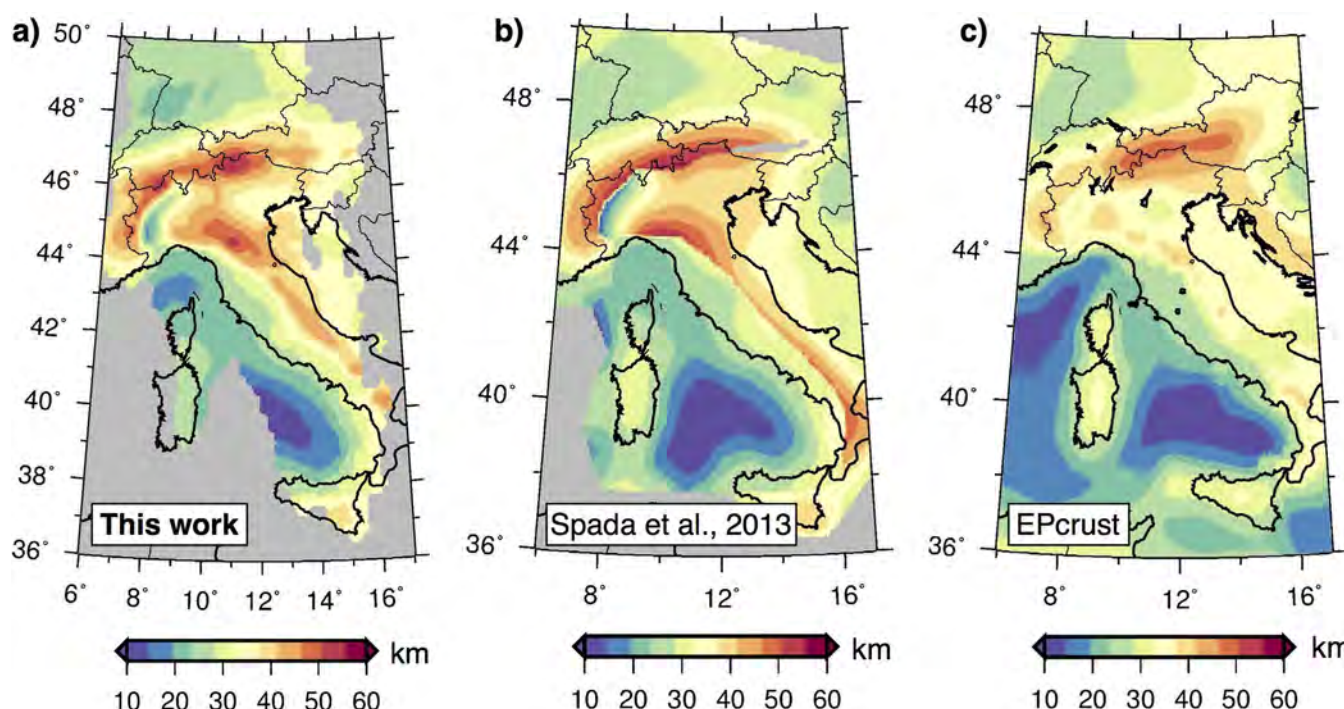


Figure 9. Comparison of the Moho depth values obtained in (a) this study, (b) Spada *et al.* [2013] and EPcrust.

crust in central Apennines (≈ 3.0 km/s). The low v_s values corresponding to the Po Plain and the North and Central Apennines can be caused by “smearing” in depth of the low surface wave velocity anomaly from 5 to 20 s (Figure 4). Within each domain, v_s does not show strong 3-D variations but highlights the difference in composition (and in origin) of Alpine and Apennines upper crust. In the southern Tyrrhenian, the crust is oceanic, the Moho depth is known to be about 10–15 km depth and low S-wave velocity values found at 10 km depth is consistent with a large percentage of partial melting and high temperature.

The 20 km deep section shows the lower crust, both in the Tyrrhenian and Adriatic domain, and the upper mantle in the Tyrrhenian sea ($v_s \approx 4.0$ km/s). Alps and Apennines show up very clearly in our imaged structure. Beneath southern Germany and north-eastern Italy, v_s is as high as 3.6–3.9 km/s. Moreover the contrast between relatively high v_s under the Tuscan Apennines and low v_s under the Marche region is in agreement with new interpretations based on the CROP3 profile [Pauselli *et al.*, 2006], which samples that area. Ligurian upper mantle is visible as high shear-speed beneath the South-Western Alps and western-most part of the Po Plain.

At 35 km depth, the geographic pattern of v_s heterogeneity is correlated with that of Moho topography. v_s values typical of the lower crust (3.6–3.9 km/s) are still found along the Alpine belt and the Northern and Central Apennines; besides that, v_s is within the range of typical upper mantle values. However, with respect to their surrounding areas, Central Apennines have relatively low v_s , i.e., between 3.2 and 3.5 km/s; this confirms published observations of anomalously low lower-crust $v_p \approx 5.8$ km/s in this region, and thus the requirement of anomalously high lower-crust temperature, given the granitic composition [Chiarabba and Amato, 1996; Chiarabba *et al.*, 2009; Di Stefano *et al.*, 2009]. Structure at larger depth (> 50 km) is not resolved well by our data set. Our data set does not allow to resolve the complex geometry of subduction zones, which should be discussed in future work involving longer-period surface-wave and/or body-wave travel-time data.

Our inversion provides also an updated Moho map since we allow crustal layer thickness to vary up to 10% with respect to the total crustal depth from the Moho of Spada *et al.* [2013]. The allowed variation is roughly within the error bar specified in the a-priori Moho. Although surface waves are only marginally sensitive to sharp discontinuities, some adjustments with respect to the a-priori Moho are expected. We show in Figure 9 the comparison between the map of Moho depth resulting from our inversion, the EPcrust one, and the

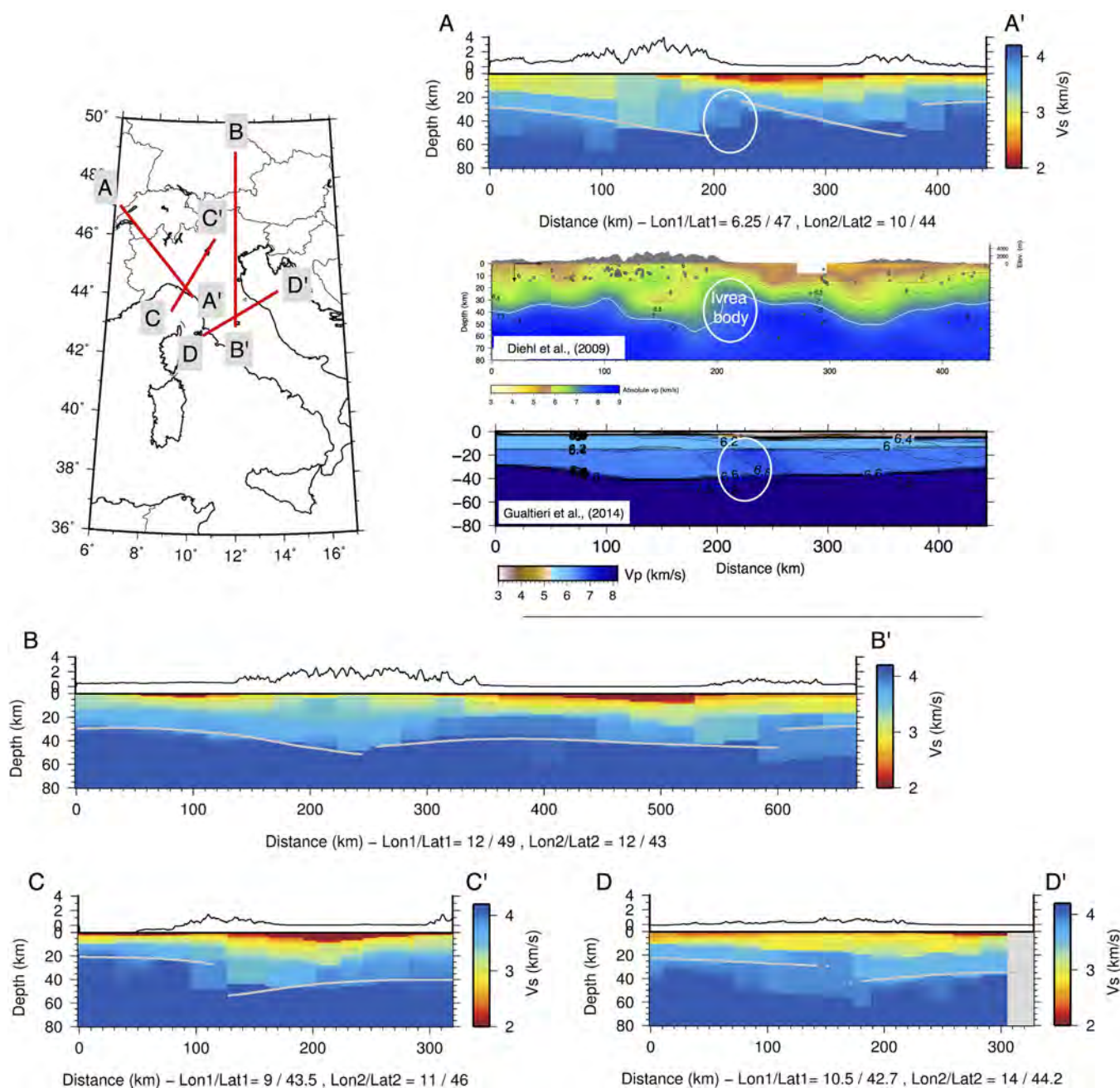


Figure 10. Vertical sections of the shear velocity model along the profiles showed in the map. The sections are not smoothed in order to well identify parameterization. In each section the Moho depth from Spada et al. [2013] is overimposed (grey line). The AA' profile (NFP-20 West section) is compared with the correspondent section from Diehl et al. [2009] and Gualtieri et al. [2014] where the Ivrea Body is identified. The BB' section is a N-S profile across the (western part of the) Eastern Alps; CC' and DD' sections document Adria-Tyrrhenian Moho suture zone.

one obtained by Spada et al. [2013] via a combination of CSS, LET and RF. Our inversion and our data set result in Moho depths from 10 to nearly 60 km, with the highest values found along the entire Alpine arc and locally beneath the Northern Apennines. These depth estimates are generally higher than those of EPcrust (Figure 9b), and in better agreement with those of Gualtieri et al. [2014]. The boundary between the Adriatic and Tyrrhenian tectonic domains appears to be defined well, with an average Moho depth of about 35–40 km in the former and about 20–30 km in the latter. Crustal thickness grows from East to West across the Western Alps. The inversion of ambient-noise data has “sharpened” the Alpine Moho with respect to EPcrust, shifting it to an overall larger depth; in the Po Plain area and throughout Adria, our final Moho

appears closer to that of EPcrust. Finally, the imaged thin Ligurian crust is similar to the results of *Spada et al.* [2013].

Vertical sections (Figure 10) of our final model reveal several prominent tectonic and geological features. These sections provide an overall view on the crustal structure and highlight the different crustal domains present in this complex region. Our model sections are not smoothed in order to well identify parameterization and to not over-interpret our results. To facilitate the discussion, on top of each section, we plot the a-priori Moho depth and, for the AA' profile (NFP-20 West section), we also show the correspondent section from *Diehl et al.* [2009] and *Gualtieri et al.* [2014] P-models. This profile is representative of the Western-Central Alps and cross the northern part of the Ivrea body [*Hunziker and Zingg*, 1980; *Rivalenti et al.*, 1975]. This feature is present in all the three works at about 200–240 km along the section and at 20–40 km depth. The similarity of models in Figure 10 is particularly significant if one considers that they have been derived using completely different data and modelling techniques, and suggests that our overall picture of this region's structure is robust. The AA' profile documents the strong variation in crustal thickness between the European crust (25–30 km), the Alpine crustal root (55 km), the strong intrusion of Ivrea body (16–20 km), the Adriatic domain (beneath the Po Plain) with 40 km of total crustal thickness and the Tyrrhenian one (25–30 km). Within the crust, the sediments and upper and lower crustal domain are clearly marked. The Po plain is a prominent feature; as explained above, the a priori model in this area is characterized a thicker-than-average sediment-layer thickness, which compensates the lack of short-period data; v_s is, however, a free parameter of the inversion (see Table 1), and, importantly, v_s values consistent with geological expectations are found within the layer. The BB' section is a N-S profile across the (western part of the) Eastern Alps, east of the Giudicaria line and goes from the Pannonian basin to the Adria-Tyrrhenia Moho suture zone, crossing the Alps, the deepest part of the Quaternary and Pliocene sediment in the Po Plain and the northern Apennines. The contrast between upper and lower crust is less pronounced in the Alpine region, indicating an almost uniform crust. The CC' and DD' sections (the latter correspond to the EE' section by *Di Stefano et al.* [2009]) show the Adria-Tyrrhenian Moho suture zone at an angle almost perpendicular to the strike of the plate boundary and illustrate the very large Moho offset that is an expression of strong ongoing tectonics.

4. Conclusions

We have derived a new 3-D v_s model that fits surface wave group and phase dispersion curves between 5 and 37 s. Virtually all other relevant data on the Italian and Alpine crust at the scale length of interest have been accounted for, in the form of an a-priori model. Especially at high frequency, our model leads to a significant reduction of surface-wave data variance, with respect to some recent crustal models. We found that, at periods between ~20 and ~40 s, both EPcrust and Crust2.0 fit our ambient-noise data fairly well, with the higher-resolution model EPcrust achieving a systematically better fit. The fact that EPcrust fits a data set that was not employed in its derivation is an important proof of its reliability.

To obtain our model, we have first inverted the database of *Verbeke et al.* [2012], to find Rayleigh-wave fundamental-mode phase- and group-velocity maps at periods from 5 to 37 s, and from 8 to 35 s, respectively. We have then applied a direct-search method (Neighbourhood Algorithm) to obtain the v_s structure under the region of interest with a nominal resolution of $0.25^\circ \times 0.25^\circ$. Our final model (i) is a complete and consistent model, including all the most relevant elastic parameters (v_p , v_s and ρ), (ii) can be considered an improvement of existing reference models like EPcrust in the Alpine and Northern Italian areas, (iii) has the same vertical parametrization of EPcrust and (iv) incorporates, as a priori information, the most recent progresses in terms of crustal structure from independent methods (LET tomography, receiver function studies and sedimentary basin modeling).

Our visual comparison with published results indicates that our model of v_s as a function of depth is physically consistent with current knowledge of v_p structure in the same region, independently obtained by other seismic methods. Tomographic maps presented here reflect the complexity of the crustal structure of the region and are highly correlated with the known surface geology features of this portion of the European crust: our 7–10 s maps are reminiscent of the geographic distribution of deep sedimentary basins, such as the Po Plan and the Molasse Basin; deeper features, including the topography of the Moho and the

three-dimensional structure of the crust under the Apennines, the Alps, Adria and the Tyrrhenian sea are resolved well by our data.

Our final preferred model consists of three layers (sediments, upper crystalline and lower crust); within each layer, the seismic parameters are described with a linear gradient. This model is suited to many applications, such as wave propagation modelling at regional scale, crustal correction in tomography, gravity studies, dynamic topography inference.

Relatively poor data fit at periods below 10 s suggests that the shallowest part of the crust, i.e., the sediment layer, is not as robustly constrained by the data as the deeper structure. Lack of resolution in shallow layers could result in trade-off and thus loss of model quality for deeper structure. In a future study, the European Plate reference crustal model may be further improved by (i) replacing its current sediment information with more detailed sediment models, and (ii) replacing its current Moho map with one of the new generation of Moho maps. In particular the sediment layers could be obtained by the integration of other sources of information, such as seismic reflection/refraction profiles, geological maps, borehole data will lead to a better definition of the shallowest properties and discontinuities within the crust.

Acknowledgments

Data to support this article are publicly available at Orfeus web site (<http://www.orfeus-eu.org/>), INGV databases (eida.rm.ingv.it); EPcrust model is available at <http://www.bo.ingv.it/eurorem/EPcrust>; CRUST2.0 model is available at <http://igppweb.ucsd.edu/gabi/crust2.html>; MAMBo model of the Po basin is available at <http://www.bo.ingv.it/molinari/MAMBo>. I.M. was partially supported by a international short visit grant of the Swiss National Science Foundation (SNSF) in 2012, and by Swiss-AlpArray Sinergia programme by SNSF. I.M. has also benefited from funding provided by the Italian Presidenza del Consiglio dei Ministri - Dipartimento della Protezione Civile (DPC). This paper does not necessarily represent DPC official opinion and policies. Figures have been prepared using the Generic Mapping tools [Wessel and Smith, 1998].

References

- Arlitt, R., E. Kissling, J. Ansorge, and T. W. Group (1999), Three-dimensional crustal structure beneath the TRO array and effects on tele-seismic wavefronts, *Tectonophysics*, 314, 309–319.
- Auer, L., L. Boschi, T. W. Becker, T. Nissen-Meyer, and D. Giardini (2014), Savani: A variable resolution whole-mantle model of anisotropic shear velocity variations based on multiple data sets, *J. Geophys. Res. Solid Earth*, 119, 3006–3034, doi:10.1002/2013JB010773.
- Baranov, A. (2010), A new crustal model for central and southern Asia, *Izv. Russ. Acad. Sci. Phys. Solid Earth*, 46(1), 34–46.
- Bassin, C., G. Laske, and G. Masters (2000), The current limits of resolution for surface wave tomography in North America, *Eos Trans. AGU*, 81, 48.
- Bensen, G. D., M. H. Ritzwoller, M. P. Barmin, A. L. Levshin, F. Lin, M. P. Moschetti, N. M. Shapiro, and Y. Yang (2007), Processing seismic ambient noise data to obtain reliable broad-band surface wave dispersion measurements, *Geophys. J. Int.*, 169(3), 1239–1260.
- Boschi, L. (2006), Global multi-resolution models of surface wave propagation: Comparing equivalently-regularized Born- and ray-theoretical solutions, *Geophys. J. Int.*, 167, 238–252.
- Boschi, L., and A. M. Dziewonski (1999), High- and low-resolution images of the Earth's mantle: implications of different approaches to tomographic modeling, *J. Geophys. Res.*, 104(B11), 25,567–25,594.
- Boschi, L., and G. Ekström (2002), New images of the earth's upper mantle from measurements of surface wave phase velocity anomalies, *J. Geophys. Res.*, 107(B4), 2059, doi:10.1029/2000JB000059.
- Boschi, L., and C. Weemstra (2015), Stationary-phase integrals in the cross correlation of ambient noise, *Rev. Geophys.*, 53, 411–451, doi:10.1002/2014RG000455.
- Boschi, L., C. Weemstra, J. Verbeke, G. Ekström, A. Zunino, and D. Giardini (2013), On measuring surface-wave phase velocity from station-station cross-correlation of ambient signal, *Geophys. J. Int.*, 192(1), 346–358.
- Bozdag, E., and J. Trampert (2008), On crustal corrections in surface wave tomography, *Geophys. J. Int.*, 172(3), 1066–1082.
- Brückl, E., et al. (2007), Crustal structure due to collisional and escape tectonics in the Eastern Alps region based on profiles Alp01 and Alp02 from the ALP 2002 seismic experiment, *J. Geophys. Res.*, 112, B06308, doi:10.1029/2006JB004687.
- Chiarabba, C., and A. Amato (1996), Crustal velocity structure of the Apennines (Italy) from P-wave travel time tomography, *Ann. Geophys.*, XXXIX(6), 1133–1148.
- Chiarabba, C., P. De Gori, and F. Speranza (2009), Deep geometry and rheology of an orogenic wedge developing above a continental subduction zone: Seismological evidence from the northern-central Apennines (Italy), *Lithosphere*, 1(2), 95–104.
- Delorey, A. A., and J. E. Vidale (2011), Basin shear-wave velocities beneath Seattle, Washington, from noise-correlation Rayleigh waves, *Bull. Seismol. Soc. Am.*, 101(5), 2162–2175.
- Diehl, T., S. Husen, E. Kissling, and N. Deichmann (2009), High-resolution 3-D P-wave model of the alpine crust, *Geophys. J. Int.*, 179(2), 1133–1147.
- Di Stefano, R., E. Kissling, C. Chiarabba, A. Amato, and D. Giardini (2009), Shallow subduction beneath Italy: Three-dimensional images of the Adriatic-European-Tyrrhenian lithosphere system based on high-quality P wave arrival times, *J. Geophys. Res.*, 114, B05305, doi:10.1029/2008JB005641.
- Doglioni, C., E. Gueguen, F. Sabat, and M. Fernandez (1999), The Western Mediterranean extensional basins and the Alpine orogen, *Terra Nova*, 9(3), 109–112.
- Dziewonski, A. M., and D. L. Anderson (1981), Preliminary reference Earth model, *Phys. Earth Planet. Inter.*, 25(4), 297–356.
- Ekström, G. (2014), Love and Rayleigh phase-velocity maps, 5–40 s, of the western and central USA from USArray data, *Earth Planet. Sci. Lett.*, 402, 42–49.
- Faccenna, C., and T. W. Becker (2010), Shaping mobile belt from small scale convection, *Nature*, 465, 602–605.
- Fry, B., F. Deschamps, E. Kissling, L. Stehly, and D. Giardini (2010), Layered azimuthal anisotropy of Rayleigh wave phase velocities in the European alpine lithosphere inferred from ambient noise, *Earth Planet. Sci. Lett.*, 297(1–2), 95–102.
- Grad, M., T. Tiira, and E. W. Group (2009), The Moho depth map of the European Plate, *Geophys. J. Int.*, 176(1), 279–292.
- Gualtieri, L., P. Serretti, and A. Morelli (2014), Finite-difference p wave travel time seismic tomography of the crust and uppermost mantle in the Italian region, *Geochem. Geophys. Geosyst.*, 15, 69–88, doi:10.1002/2013GC004988.
- Handy, M. R., S. M. Schmid, R. Bousquet, E. Kissling, and D. Bernoulli (2010), Reconciling plate-tectonic reconstructions with the geological-geophysical record of spreading and subduction in the Alps, *Earth Sci. Rev.*, 102, 121–158.
- Hansen, P. C. (1992), Analysis of discrete ill-posed problems by means of the l-curve, *SIAM Rev.*, 34(4), 561–580.
- Hunziker, J. C., and A. Zingg (1980), Lower Paleozoic amphibolite to granulite facies metamorphism in the Ivrea Zone (Southern Alps, Northern Italy), *Schweiz. Mineral. Petrogr. Mitt.*, 60, 181–213.

- Husen, S., T. Diehl, and E. Kissling (2009), The effects of data quality in local earthquake tomography: Application to the Alpine region, *Geophysics*, 74(6), WCB71–WCB79.
- Kao, H., Y. Behr, C. A. Currie, R. Hyndman, J. Townend, F.-C. Lin, M. H. Ritzwoller, S.-J. Shan, and J. He (2013), Ambient seismic noise tomography of Canada and adjacent regions: Part I. Crustal structures, *J. Geophys. Res.*, 118, 5865–5887, doi:10.1002/2013JB010535.
- Lebedev, S., J. M.-C. Adam, and T. Meier (2013), Mapping the Moho with seismic surface waves: A review, resolution analysis, and recommended inversion strategies, *Tectonophysics*, 609, 377–394.
- Li, H., F. Bernardi, and A. Michelini (2010), Surface wave dispersion measurements from ambient seismic noise analysis in Italy, *Geophys. J. Int.*, 180(3), 1242–1252.
- Lin, F., M. Moschetti, and M. Ritzwoller (2008), Surface wave tomography of the western United states from ambient seismic noise: Rayleigh and Love wave phase velocity maps, *Geophys. J. Int.*, 173(1), 281–298.
- Meier, T., K. Dietrich, B. Stöckhert, and H.-P. Harjes (2004), One-dimensional models of shear wave velocity for the eastern Mediterranean obtained from the inversion of Rayleigh wave phase velocities and tectonic implications, *Geophys. J. Int.*, 156(1), 45–58.
- Molinari, I., and A. Morelli (2011), EPCrust: A reference crustal model for the European plate, *Geophys. J. Int.*, 185(1), 352–364.
- Molinari, I., V. Raileanu, and A. Morelli (2012), A crustal model for the Eastern Alps region and a new Moho map in South-Eastern Europe, *Pure Appl. Geophys.*, 169(9), 1575–1588.
- Molinari, I., A. Argnanì, A. Morelli, and P. Basini (2015), Development and testing of a 3D seismic velocity model of the Po Plain sedimentary basin, Italy, *Bull. Seismol. Soc. Am.*, 15(2a).
- Paige, C., and M. Saunders (1982), LSQR: An algorithm for sparse linear equations and sparse least squares, *Trans. Math. Software*, 8(1), 43–71.
- Pauselli, C., M. R. Barchi, C. Federico, M. B. Magnani, and G. Minelli (2006), The crustal structure of the Northern Apennines (Central Italy): an insight by the CROP03 seismic line, *Am. J. Sci.*, 306(6), 428–450.
- Piana Agostinetti, N., and A. Amato (2009), Moho depth and Vp/Vs ratio in peninsular Italy from teleseismic receiver functions, *J. Geophys. Res.*, 114, B06303, doi:10.1029/2008JB005899.
- Piromallo, C., and A. Morelli (2003), P wave tomography of the mantle under the Alpine-Mediterranean areas, *J. Geophys. Res.*, 108(B2), 2065, doi:10.1029/2002JB001757.
- Ritzwoller, M. H., and A. L. Levshin (1998), Eurasian surface wave tomography: Group velocities, *J. Geophys. Res.*, 103(B3), 4839–4878.
- Rivalenti G., G. Garuti, and A. Rossi (1975), The origin of the Ivrea-Verbano basic formation (Western Alps) - Whole rock geochemistry, *Bol. Soc. Geol. Ital.*, 94, 1149–1186.
- Sambridge, M. (1999a), Geophysical inversion with a Neighbourhood Algorithm-I. Searching a parameter space, *Geophys. J. Int.*, 138(2), 479–494.
- Sambridge, M. (1999b), Geophysical inversion with a Neighbourhood Algorithm-II. Appraising the ensemble, *Geophys. J. Int.*, 138(2), 727–746.
- Saygin, E., and B. L. N. Kennett (2012), Crustal structure of Australia from ambient seismic noise tomography, *J. Geophys. Res.*, 117, B01304, doi:10.1029/2011JB008403.
- Schivardi, R., and A. Morelli (2011), Epmantle: A 3-D transversely isotropic model of the upper mantle under the European Plate, *Geophys. J. Int.*, 185(1), 469–484.
- Schmid, S.M., and E. Kissling (2000), The arc of the Western Alps in the light of geophysical data on deep crustal structure, *Tectonics*, 19(1), 62–85.
- Serretti, P., and A. Morelli (2011), Seismic rays and traveltimes tomography of strongly heterogeneous mantle structure: Application to the central Mediterranean, *Geophys. J. Int.*, 187(3), 1708–1724.
- Shapiro, N. M., and M. H. Ritzwoller (2002), Monte-Carlo inversion for a global shear-velocity model of the crust and upper mantle, *Geophys. J. Int.*, 151, 88105.
- Shapiro, N. M., M. Campillo, L. Stehly, and M. H. Ritzwoller (2005), High-resolution surface-wave tomography from ambient seismic noise, *Science*, 307(5715), 1615–1618.
- Snieder, R. (2004), Extracting the Green's function from the correlation of coda waves: a derivation based on stationary phase, *Phys. Rev. E*, 69, 046610.
- Solarino, S., E. Kissling, M. Cattaneo, and C. Eva (1997), Local earthquake tomography of the southern part of the Ivrea body, North-Western Italy, *Eclogae Geol. Helv.*, 90, 357–364.
- Spada, M., I. Bianchi, E. Kissling, N. Piana Agostinetti, and S. Wiemer (2013), Combining controlled-source seismology and receiver function information to derive 3-D Moho topography for Italy, *Geophys. J. Int.*, 194(2), 1050–1068.
- Stehly, L., B. Fry, M. Campillo, N. M. Shapiro, J. Guilbert, L. Boschi, and D. Giardini (2009), Tomography of the Alpine region from observations of seismic ambient noise, *Geophys. J. Int.*, 178(1), 338–350.
- Tesauro, M., M. K. Kaban, and S. A. P. L. Cloetingh (2008), EuCRUST-07: A new reference model for the European crust, *Geophys. Res. Lett.*, 35, L05313, doi:10.1029/2007GL032244.
- Verbeke, J., L. Boschi, L. Stehly, E. Kissling, and A. Michelini (2012), High-resolution Rayleigh-wave velocity maps of central Europe from a dense ambient noise dataset, *Geophys. J. Int.*, 188(3), 1173–1187.
- Wagner, M., E. Kissling, and S. Husen (2012), Combining controlled-source seismology and local earthquake tomography to derive a 3-D crustal model of the western Alpine region, *Geophys. J. Int.*, 191(2), 789–802.
- Waldhauser, F., E. Kissling, J. Ansorge, and S. Mueller (1998), Three-dimensional interface modelling with two-dimensional seismic data: The alpine crust-mantle boundary, *Geophys. J. Int.*, 135, 264–278.
- Warren, L. M., S. L. Beck, C. B. Biryol, G. Zandt, A. A. Özacar, and Y. Yang (2013), Crustal velocity structure of Central and Eastern Turkey from ambient noise tomography, *Geophys. J. Int.*, 194(3), 1941–1954.
- Wathelet, M. (2008), An improved neighborhood algorithm: Parameter conditions and dynamic scaling, *Geophys. Res. Lett.*, 35, .
- Wessel, P., and W. H. F. Smith (1998), New, improved version of the Generic Mapping Tools released, *Eos Trans. AGU*, 79, 579.
- Zulfakriza, Z., E. Saygin, P. R. Cummins, S. Widiyantoro, A. D. Nugraha, B.-G. Lühr, and T. Bodin (2014), Upper crustal structure of central Java, Indonesia, from transdimensional seismic ambient noise tomography, *Geophys. J. Int.*, 197(1), 630–635.